

Regular vs. chaotic mantle mixing

Sylvaine Ferrachat¹, Yanick Ricard^{*}

École Normale Supérieure de Lyon, 46 allée d'Italie, F-69364 Lyon Cedex 07, France

Received 17 March 1997; revised 11 September 1997; accepted 30 October 1997

Abstract

Most quantitative models of mantle mixing have been based on simulations of tracer advection by 2-D flows. The present work shows that the mixing properties of 3-D time-independent flows cannot be understood or extrapolated from previous 2-D models. Steady convective flows appropriate to simulate a uniform fluid with large viscosity are restricted to poloidal components. They seem to have regular streamlines. However, the existence of plates on the Earth's surface imposes the existence of a strong toroidal field. Flows where both poloidal and toroidal components are present can yield chaotic pathlines which are very efficient in mixing the mantle. Within areas of turbulent mixing where the stretching increases exponentially with time, regular islands of laminar stretching persist in which unmixed material can survive. Our findings indicate that the intrinsic three-dimensionality of convection coupled with plates as much as its time dependence must be included in numerical models to understand the mixing properties of the mantle. As the viscosity is significantly larger in the lower mantle than in the upper mantle, the toroidal component of the flow is confined to the upper mantle, where a more thorough mixing should take place. © 1998 Elsevier Science B.V.

Keywords: convection; mantle; mixing; three-dimensional models

1. Introduction

Mantle geochemical heterogeneities are created at shallow level by partial melting under ridges and erosion/sedimentation processes. These heterogeneities, frozen in the cooling oceanic lithosphere, are ultimately destroyed by mantle convection. Samples from the mantle are extracted at ridges and hotspots. Their elemental and isotopic composition suggests the existence of various geochemical reser-

voirs at depth (e.g., [1–4]). One of them, the MORB reservoir, is well mixed and is the source of ridge basalts. The isotopic heterogeneity of other reservoirs shows that they have been isolated for billion years. Understanding the rehomogenization and mixing in the mantle is thus fundamental for interpreting these observations.

As diffusion in solid phases is very slow even at mantle temperature, material heterogeneities must be thinned down to meter size before diffusion becomes efficient. Therefore, the behavior of heterogeneities can be studied from models where tracers are simply advected. The pathline of a tracer reads

$$\frac{dx_i}{dt} = u_i \quad (1)$$

^{*} Corresponding author. Fax: 33 4 72 72 86 77. E-mail: ricard@geologie.ens-lyon.fr

¹ Fax: +33-4-72-72-86-77; E-mail: sferrach@geologie.ens-lyon.fr

where t is the time, $x_i(t)$ are the coordinates of the tracer and u_i are the velocity components. Various papers have studied the implications of Eq. (1) for geochemistry. What has been done to simulate the mantle circulation in 2-D models where the flow is induced by imposing plate-like velocities at the surface, is computed by a 2-D convection code, or both (e.g., [5–9]). Previous work has generally assumed that the tracers are passive, i.e. have mechanical properties comparable with those of the surrounding mantle. In that case, the background velocity is independent of the distribution of tracers. More recently, this assumption of passive tracers has been removed in 2-D studies where the entrained bodies have different viscosities [10] or densities [11]. Tackling the problem of the mixing properties of the mantle using a 3-D flow has been addressed only by Gable et al. [12] and Schmalzl et al. [13,14].

2. Considerations on the flow pattern

Assuming that the mantle is incompressible, the mass conservation equation allows us to express in the most general way the velocity field into two components. They are known as the poloidal (or spheroidal) and toroidal components and can be deduced from two 3-D scalar fields P and T . The general form of Eq. (1) on Cartesian coordinates with z vertical, reads:

$$\frac{dx}{dt} = \frac{\partial T}{\partial y} + \frac{\partial^2 P}{\partial z \partial x} \quad (2a)$$

$$\frac{dy}{dt} = -\frac{\partial T}{\partial x} + \frac{\partial^2 P}{\partial z \partial y} \quad (2b)$$

$$\frac{dz}{dt} = -\frac{\partial^2 P}{\partial x^2} - \frac{\partial^2 P}{\partial y^2} \quad (2c)$$

The poloidal flow has a 3-D structure without vertical vorticity, the toroidal flow corresponds to rotations in the horizontal plane. In spherical coordinates the poloidal flow has no radial vorticity, the toroidal flow is confined on spherical shells. In other words, the surface expressions of the mantle poloidal flow are ridges and trenches, the surface expressions of the toroidal flow are strike-slip faults.

This differential system is somewhat akin to the

Hamiltonian system of classical mechanics. When the flow is only two-dimensional, system (2) is equivalent to a Hamiltonian system with one degree of freedom in the steady case. This means that a conserved quantity can be defined, or equivalently, that the velocities are perpendicular to the equipotentials of a stream-function. For example, when the flow is confined to the xy plane, T is conserved. In a steady flow, the pathlines described by the tracers also correspond to streamlines. Therefore, in 2-D time-independent flows, the trajectories are closed loops that tracers follow indefinitely.

In the 3-D case, the larger dimensionality of system (2) could lead to a much more complex dynamics. This system can be shown to be equivalent to a two-degrees-of-freedom Hamiltonian (e.g., [15,16]). In this case one can expect that the system will yield a chaotic behavior even in the case of a steady flow. For example, the so-called ABC flows [17], other space periodic flows [18] or bounded flows [19,20] are steady flows yielding chaotic pathlines. While these flows are quite idealized and are not appropriate for the Earth mantle, they give a glimpse on the intricacy of chaotic and regular regions in 3-D flows.

In the case of Rayleigh–Bénard convection, chaos is present at finite Prandtl number [21]. Contrarily, Schmalzl et al. [13] have found that 3-D steady-state convection at infinite Prandtl number is associated with a non-chaotic behavior. In their numerical experiments the tracers are found to be confined at the surface of tori. The intersections of these tori by planes define closed loops. The trajectory of a tracer at the surface of a torus can either be periodic or may densely fill the surface of the torus. Even in this case, the strong confinement of the trajectories forbids an efficient mixing.

Schmalzl et al. [13] used a convection model at infinite Prandtl number and with constant viscosity. In this case, it can be shown that the toroidal field T of Eqs. 2, is zero (e.g., [22]). It seems thus that, although kinematically imposed 3-D flows could induce chaotic pathlines [19] even when they are reduced to poloidal components [20], 3-D poloidal flows which are solutions of convection equations at infinite Prandtl number and with free surface conditions cannot. In the case of thermal convection, the presence of toroidal motion, either naturally excited

at low Prandtl number [21] or kinematically imposed [19], can be the cause of chaotic motions.

At the surface of the Earth, the poloidal and toroidal components of motion have been roughly equal for tens of million years [23–25] as the consequence of the existence of rigid and independent tectonic plates. The problem of mixing in the mantle has never been studied in a regime where kinetic energies described by the poloidal and toroidal components are comparable.

3. A simple flow pattern

In this paper, we consider a circulation model driven by surface motions only. We use a 3-D Cartesian geometry and confine the flow to a box of square horizontal section whose depth H is two-thirds of the section width L . To excite both poloidal and toroidal flows, the surface is divided into two rigid plates. The two plates are separated by a “transform fault” and two “ridges”. The two ridges have the same length equal to $L/2$. Each plate has a constant and uniform velocity parallel to the transform fault. We impose free slip conditions at the bottom of the box and reflecting boundary conditions on the four lateral faces. Therefore, the boundary at the front simulates a “subduction”. This very simple geometry is described in Fig. 1 in a case where one plate remains fixed. A schematic view of the flow imposed at the surface and computed at the front and the right-hand sides of the box is also depicted.

The numerical solution for the induced 3-D cavity flow can be easily found through a Fourier transform in the horizontal directions. The vertical variations of the flow are obtained by means of a classic propagator method [26]. The velocity flow is computed on a $128 \times 128 \times 129$ grid. Within each element, the velocity components are interpolated from the eight closest neighbors using a trilinear scheme. We define the poloidal and toroidal amplitudes σ_P and σ_T of a flow by

$$\sigma_P^2 = \int \left[\left(\frac{\partial^2 P}{\partial z \partial x} \right)^2 + \left(\frac{\partial^2 P}{\partial z \partial y} \right)^2 \right] dx dy \quad (3a)$$

$$\sigma_T^2 = \int \left[\left(\frac{\partial T}{\partial y} \right)^2 + \left(\frac{\partial T}{\partial x} \right)^2 \right] dx dy \quad (3b)$$

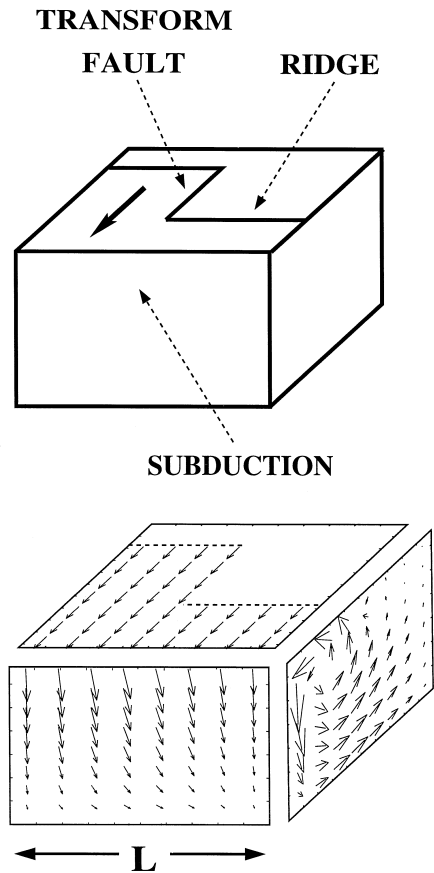


Fig. 1. Box of aspect ratio 2/3 in which the computation is performed. The flow is only driven by a surface motion mimicking a real plate with a segmented ridge, a transform fault and a subduction zone (top). The resulting flows at the surface, the front and the right-hand faces are depicted at the bottom.

respectively, where the integrals are computed on the top surface of the box. We can modify the toroidal/poloidal ratio of the flow, σ_T/σ_P , by modifying the length of the transform fault. When no transform fault is present, the flow field is purely 2-D and poloidal. When the length of the transform fault is L , the toroidal field attains its maximum amplitude but a poloidal component still exists. Indeed, the reflecting boundary conditions impose a subduction on the front face of the box and a ridge on the back face. With this geometry, the ratio between toroidal and poloidal amplitudes reaches 58%.

In the computation of the flow, poloidal and toroidal velocity components decouple. Therefore,

for a given choice of surface plate motion, we can also study the effects of the two components separately or by adding them in variable proportions. The velocity fields that can be obtained by arbitrarily mixing the two components satisfy the boundary conditions of zero normal velocity on the faces of the box and of free slip at the vertical faces and at the bottom of the box. However, the composite surface velocity does not correspond to the motion of rigid plates anymore, unless the two components are in the same proportion as in the original case.

4. Regular and chaotic behavior

When the computation of the three velocity components u_i is done, the motions of tracers are com-

puted from the advection equation (1). The advection equation is solved by a fifth-order step-adaptive Runge–Kutta method. As the pathlines may be very complex in 3-D, we resort to Poincaré mapping, i.e., we simply consider the successive intersections between a pathline and a fixed plane that we choose as horizontal and located at mid-depth of the box.

Fig. 2 depicts various experiments made with different geometries where the length of the transform fault is varied from 0 (Fig. 2a) to L (Fig. 2f). The corresponding toroidal/poloidal ratios are 0%, 11%, 23%, 32%, 47% and 58%. The plate geometries and surface motions (one fixed, one moving) are indicated with dashed lines. Only a few tracers are followed in their motions and each tracer is represented by a different color. The number of tracers, their initial positions and the total duration of

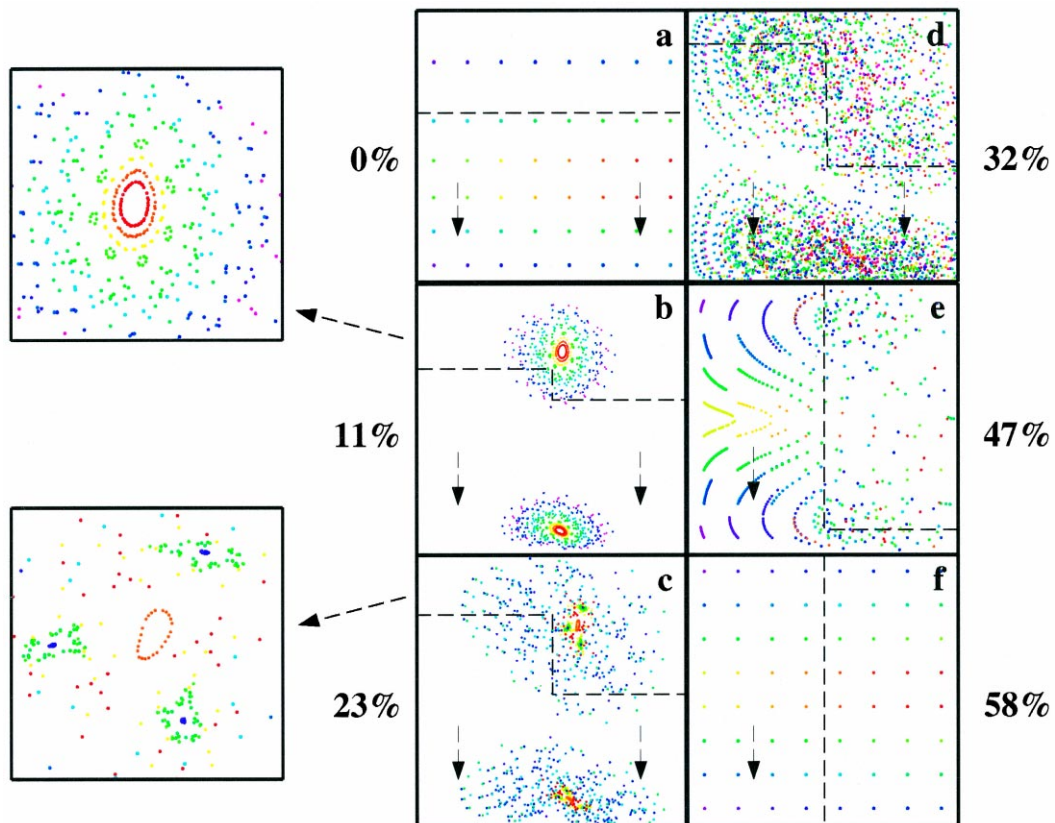


Fig. 2. Poincaré sections obtained by plotting the intersections of the pathlines of ~ 50 tracers with the horizontal mid-depth plane. Each tracer has its own color. The shapes of the surface velocities are indicated by *dashed lines*. The values of the toroidal/poloidal ratios are given in %. Two sections (b) and (c) are blown up for details and are depicted on the left-hand side. The transition from (a) to (d) is associated with an increase in the ergodicity of the pathlines.

the advection are for the moment, without importance. They have been chosen only to highlight the geometry of the Poincaré sections. Although the flow pattern is merely a simple roll in all the experiments, the behaviors of the pathlines change drastically with the length of the transform fault.

When the flow is purely poloidal and 2-D (Fig. 2a), the trajectories are closed loops in vertical planes perpendicular to the ridge. Thus, the Poincaré section for each tracer consists of only a couple of points (in Fig. 2a, 24 tracers are followed and give rise to 24 couples of points). When the toroidal component has a small amplitude (Fig. 2b), the Poincaré section reveals, at least locally, regular motions mapped through concentric loops. This indicates that the tracers orbit on the surface of embedded tori. The axis of the tori are parallel to the ridges. The tracers are crossing the mid-depth plane going upward below the fixed plate and downward below the moving plate. Regular island chains are also observed between loops. For example, a green tracer draws a 7-island chain in the blow-up of Fig. 2b. These islands are cross-sections of invariant tubes winding between the tori.

When the toroidal/poloidal ratio increases, the domain of regular motions with loops and island chains decreases in size. In the case of Fig. 2c, only a very small region of loops surrounded by a 3-island chain persists (see blow-up of Fig. 2c). A further increase in the toroidal/poloidal ratio (Fig. 2d) apparently destroys all regularity in the pathlines. When the transform fault is even longer (Fig. 2e), the pathlines regain some regularity as the poloidal flow itself becomes less twisted. In the extreme case where the transform fault cuts the surface into two rectangular plates (Fig. 2e), the Poincaré sections reduce to couples of points. The trajectories are again closed loops although they are bent and do not lie on vertical planes like those of the case of Fig. 2a.

The numerical experiments depicted in Fig. 2 suggest a relationship between the variations of the toroidal/poloidal ratio and the amount of ergodicity in the pathlines. The evolution of the topology of the Poincaré sections (Fig. 2a–d) is indeed comparable with the well-known transition to chaos for near-integrable Hamiltonian systems [27–29]. The regions close to elliptic points (i.e., surrounded by closed

loops) are stable under the effect of a perturbation whereas the tracers start wandering erratically next to the hyperbolic points (i.e., between two islands). The invariant structures of low periodicity are the most stable: as the percentage of toroidal/poloidal ratio increases, more and more winding tubes and more and more tori are destroyed until the flow appears ergodic.

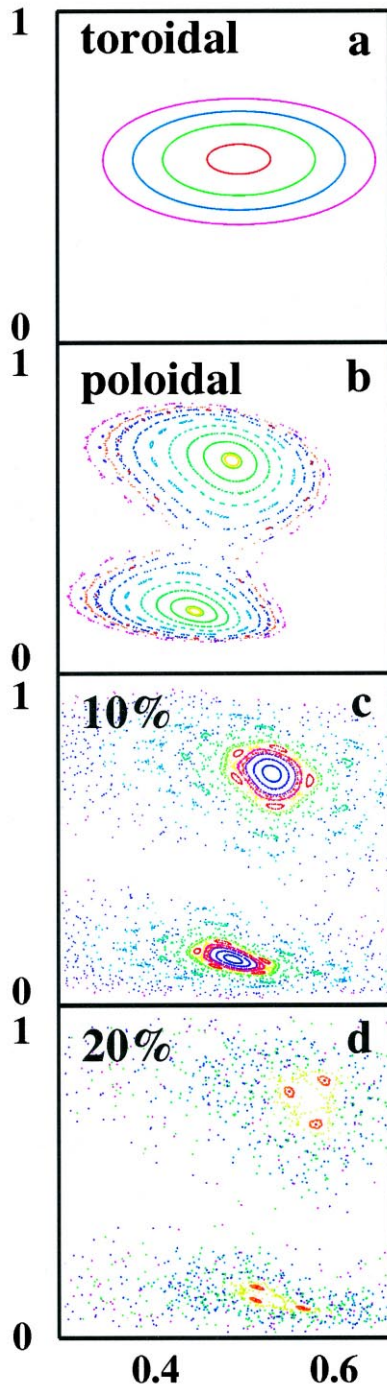
However, the transition observed from Fig. 2d–f shows that the presence of a large amount of vertical vorticity in addition to a poloidal flow does not forbid the existence of regular pathlines. This indicates that the poloidal field, by itself, must be complex enough to be associated with chaotic pathlines. One thus wonders whether the changes in the Poincaré sections of Fig. 2a–f may not be related rather to an increase in the complexity of the poloidal field, reaching a maximum in Fig. 2d, than to the presence of a toroidal component.

In order to test this hypothesis we consider separately the poloidal and toroidal components of the flow field corresponding to the case of Fig. 2d and add them in variable proportions before computing the Poincaré sections. These numerical experiments allow us to verify that the transition from regular to chaotic pathlines is not simply due to the changes in the geometry of each velocity component.

In Fig. 3, we have mixed the toroidal and poloidal components present in the flow corresponding to Fig. 2d. In Fig. 3a, the flow is purely toroidal, in Fig. 3b, purely poloidal, in Fig. 3c and d, the toroidal/poloidal ratio is 10% and 20%, respectively. Adding the two flows with a ratio of 32% would again lead to the Poincaré section depicted in Fig. 2d. In the presence of the purely toroidal field (Fig. 3a), the pathlines are very simple. As seen from inspection of Eqs. 2, the motions are only 2-D (the vertical velocity is zero) and the pathlines are closed concentric horizontal loops (the isolines of T) and they coincide with the Poincaré sections. In Fig. 3b, the flow corresponds to the poloidal field alone. In this case, the Poincaré section shows regular structures. If the pathlines in a purely poloidal field correspond to the dynamics of an integrable Hamiltonian system, any perturbation may destroy the stability of the structures of highest periodicity. We think that the wiggles and islands drawn in the outer loops of the Poincaré section of Fig. 3b reveal the

existence of perturbations inherent to the numerical treatment of the problem.

Addition of some toroidal components (Fig. 3c



and d) partly destroys the regularity of the sections. The transition between regularity and ergodicity already observed when the length of the transform fault is increased is again found with the same gradual destruction of tori and of island chains of large periodicity. Thus, for our cavity flow, the presence of a toroidal field seems to be necessary to obtain a large domain of chaotic pathlines. Its absence explains why only regular structures are found in the numerical experiments of Schmalzl et al. [13].

5. Implications for mantle mixing

For a 2-D steady flow, heterogeneities are trapped by closed pathlines, the mixing is inefficient and each streamline behaves as an isolated “geochemical reservoir”. In the time-dependent case, the mixing rate is related to the explicit time dependence of the flow but the problem is to keep unmixed reservoirs as requested by geochemical observations.

The characteristics of the 3-D steady mixing are drastically different and depend upon the poloidal flow complexity and the toroidal/poloidal ratio of the flow. Fig. 4 depicts the general topology of the invariant surfaces when the toroidal component has a vanishing amplitude as revealed by the Poincaré sections of Figs. 2 and 3. The tracers are spiraling on the various surfaces, either as tori (dark grey) or tubes, like the one light-grey winding five times around the inner torus. According to the ratio between the periodicities of a tracer around the small and large radii of the tori (rational or irrational), these surfaces can be densely filled or not. The mixing occurs slowly and at most on a 2-D surface. As heterogeneities remain confined on nested surfaces, an infinite number of isolated reservoirs are present.

With a small percentage of toroidal flow, some invariant tori are preserved but between them, the

Fig. 3. Poincaré sections obtained for various 3-D flows obtained by arbitrarily mixing the poloidal and toroidal components present in Fig. 2d. In (a), the flow is only toroidal, in (b) poloidal. The toroidal/poloidal ratios are 10% and 20% in (c) and (d), respectively. Whereas the sections obtained for either a pure toroidal or a pure poloidal flow [(a) and (b)] are regular, chaotic regions develop in (c) and (d).

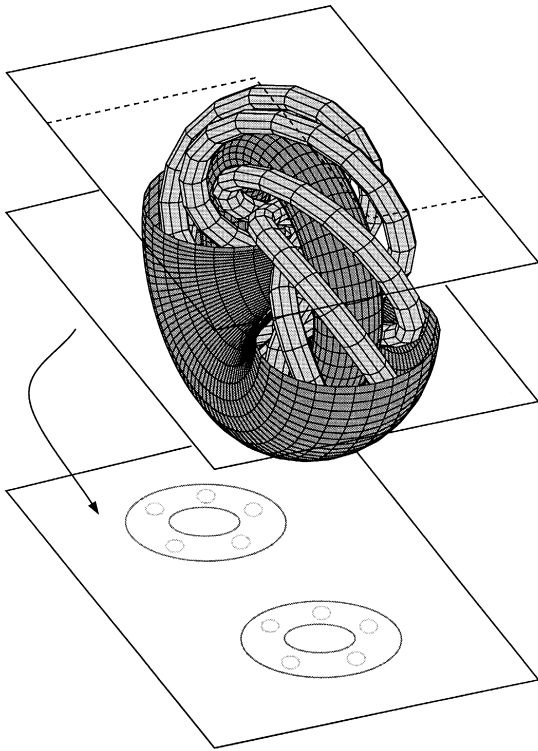


Fig. 4. Topology of the pathlines obtained for a pure poloidal field. The tracers are spiraling around the tori and tubes. The intersection of pathlines by a plane gives rise to the loops and island chains seen in Fig. 2. Fig. 3. Adding some toroidal components breaks tubes, then tori.

pathlines start wandering. The flow topology consists of stable tori like the dark-grey surfaces in Fig. 4, but some light-grey tubes are destroyed, yielding 3-D impermeable but mixed reservoirs. The presence of segregated stable tubes coexisting with chaotic advection has also been observed experimentally in other steady flows with different geometries [18]. Above some threshold for the toroidal energy, all tori seem to be destroyed and the whole box corresponds to a single reservoir.

It seems intuitive that the efficiency of mixing should be the fastest in regions where the flow is chaotic. However, this is not necessarily true, as mixing efficiency is not only related to stretching but also to reorientation and folding of the streak-lines. In addition, during the computations of the Poincaré sections, we never compare the duration of the advection experiment with the characteristic return time of mantle convection. In Fig. 3b for example, a

tracer belonging to the outermost loops has performed some 150 overturns. This is probably from 2 to 20 times the number of overturns a mantle heterogeneity can experience in the whole history of the Earth not withstanding the obvious fact that the mantle flow is certainly not steady. The above advection experiments are only meant to reveal the behavior of a flow.

Computing the Lyapunov exponents is far more illustrative than discussing Poincaré sections to understand the implications of pathline ergodicity on mantle mixing. The Lyapunov exponents are related to local stretching. If X is the length of a vector \vec{X} located at the position M and $X(t)$ its length after a time t , the Lyapunov exponent $\sigma(M, \vec{X})$ is defined by

$$\sigma(M, \vec{X}) = \lim_{\substack{t \rightarrow \infty \\ X \rightarrow 0}} \left[\frac{1}{t} \ln \left(\frac{X(t)}{X} \right) \right] \quad (4)$$

In a 3-D incompressible flow, there are three Lyapunov exponents at each point and their sum is zero. The existence of at least one strictly positive exponent (at most two) is a mark of chaos. This means that the stretching undergone by a tracer increases asymptotically as an exponential function of time. This phenomenon is also called turbulent mixing whereas the cases in which the Lyapunov exponents are zero (e.g., when the stretching increases linearly with time) correspond to laminar mixing [30]. Computing the three exponents in a 3-D flow is complex. However, computing the largest one is much easier when one realizes that any arbitrary \vec{X} likely has a non-zero component along the eigenvector associated with the largest Lyapunov exponent and therefore will stretch at a rate controlled by this exponent.

Practically, we follow the distance between two very close tracers and renormalize this distance periodically. The Lyapunov exponent that we obtain is certainly neither obtained for an infinitely small starting vector nor for an infinite time as would be implied by Eq. (4). It is preferable to call it a finite-time Lyapunov exponent [28]. The numerical computation of a non-zero exponent cannot be taken as a proof of chaoticity as even linear stretching would yield a non-zero finite-time Lyapunov exponent. The finite-time Lyapunov exponents have been

computed for tracers located at mid-depth of the box and the local stretching has been followed during 100 transit times; a transit time being the box depth divided by the plate velocity.

Fig. 5 depicts the Lyapunov exponents computed in four different cases and plotted at the starting positions of the 240^2 tracers. The blue color corre-

sponds to low exponents. The reader must realize that the color homogeneity in the blue areas is associated with low stretching rates and therefore with mantle heterogeneity. In contrast, the areas of visually heterogeneous green to red colors are associated with a well-mixed mantle. On the top part of the figure (Fig. 5a and b), the flow is purely poloidal.

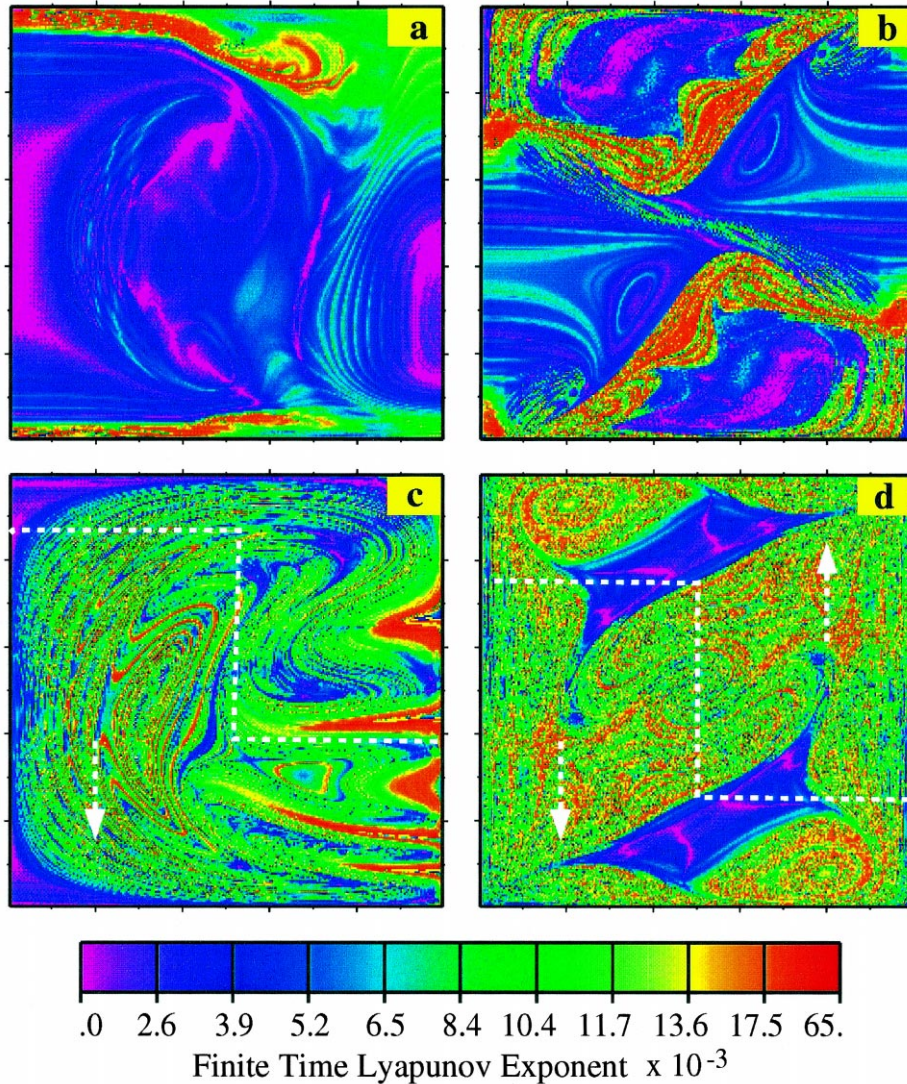


Fig. 5. Finite-time Lyapunov exponents for tracers initially located at mid-depth in the box. The flows are either poloidal (*top*) or correspond to cavity flows induced by rigid plates (*bottom*). In the left-hand column only one plate is moving whereas the two plates are moving in opposite directions in the right-hand column as shown in the bottom row. The differences between regular and chaotic regions are obvious. The large area of laminar mixing shrinks when toroidal components are present. Islands of laminar mixing can coexist with ergodic regions (d).

The left-hand panel (Fig. 5a) corresponds to the poloidal part of the flow induced by only one plate moving with velocity V . The flow is thus the same as what led to the Poincaré section of Fig. 3b. In the right-hand panel (Fig. 5b), the flow corresponds to the poloidal part of the velocity obtained when the two plates are moved in opposite directions at the same velocity V . For the flows induced by the motion of rigid plates (poloidal and toroidal components together), the Lyapunov exponents are depicted in the bottom part. In Fig. 5c, only one plate moves. This corresponds to the case already studied in Fig. 2d. In Fig. 5d the two plates move in opposite directions. We scale the velocity flows in the poloidal cases to have the same surface kinetic energy than in their toroidal/poloidal counterparts. Plotting the Lyapunov exponents at the starting positions of the advected tracers rather than at the ending positions is arbitrary but easier: in the latter case the data would not have been regularly spaced on a grid. We verified however that comparable figures are obtained when the Lyapunov exponents are plotted at the ending positions.

The scale is in units of V/H , in other words a Lyapunov exponent of 0.0175, means that the rela-

tive stretching is of the order $e^{0.0175} = 1.018$ every H/V time. Taking $H = 670$ km and $V = 10$ cm/yr, a 7 km thick oceanic crust located in a spot where the Lyapunov exponent is larger than 0.00175 is reduced to 10 cm in less than 4.2 Gyr. This stretching rate may seem low but is in fact fast for a steady-state flow; it is also comparable with what is inferred from field and geochemical observations by Allègre and Turcotte [31]. However, scaling this toy model to the real Earth is rather arbitrary as the mixing properties have a strong dependency on the details of the flow pattern [32].

The differences between the Lyapunov exponents computed for purely poloidal flows (Fig. 5a and b) and plate driven flows (Fig. 5c and d) are obvious. The exponents are on average much larger in the plate driven flows than in the purely poloidal flows; the presence of the toroidal component enlarges the ergodic areas. The areas of chaoticity are sheeted. Even in the pure poloidal cases some seemingly chaotic zones exist. This observation is puzzling. It seems to contradict the conclusions of Arter [21] or Schmalzl et al. [13] which suggest the inexistence of pathline chaoticity in Rayleigh–Bénard convection with infinite Prandtl number, i.e., when the flow is

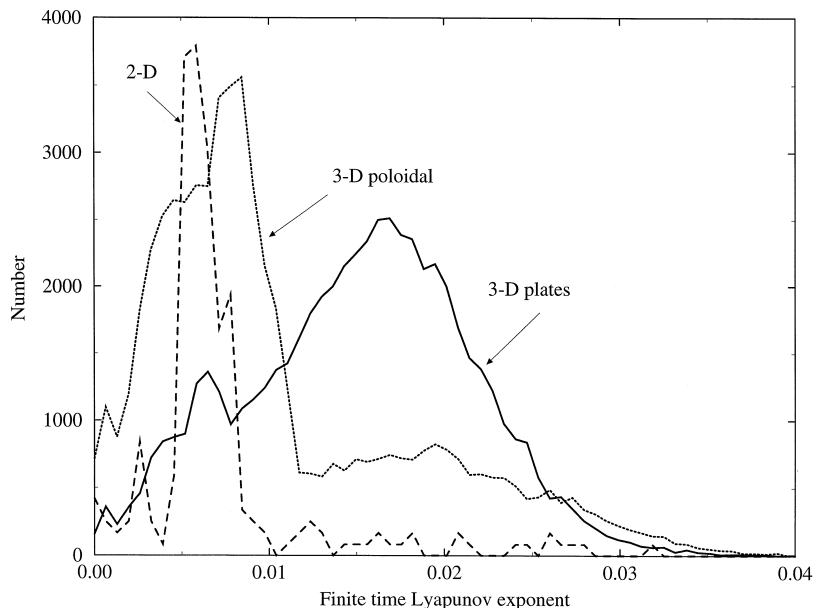


Fig. 6. Histograms of the finite-time Lyapunov exponents seen in Fig. 5c and d. An histogram of the values obtained in the case of a pure 2-D poloidal field (a simple ridge without transform fault) is also depicted. The exponents of the 2-D case and the 3-D poloidal case are comparable. The existence of plates leads to larger exponents (curve labeled “3-D plates”).

only poloidal. We are aware however, that the computed 3-D cavity flow does not correspond to the convection pattern of a fluid with uniform viscosity. Flows induced by plates, although presenting mostly chaotic regions can also exhibit regular areas. In Fig. 5d, the blue areas of near-zero Lyapunov exponents are enclosed by very sharp boundaries.

Fig. 6 depicts an histogram of the Lyapunov exponents obtained with three different flow patterns having the same surface kinetic energy. The curve labeled “2-D” is for the purely 2-D poloidal case of Fig. 2a. In this case we know that the pathlines are regular, that the stretching is linear rather than exponential and that the computation of non-zero Lyapunov is only due to the finite duration of the experiment. The curves labeled “3-D plates” and “3-D poloidal” are obtained when the flow is induced by symmetrically divergent plates and by the restriction of this flow to its poloidal component. The histogram for the 3-D poloidal case has roughly the same average as the 2-D case. The flow induced by plates is associated with ~ 3 times larger exponents.

6. Conclusions

In previous works, steady-state Rayleigh–Bénard convection flows were apparently unable to generate Lagrangian chaos at infinite [13] or large Prandtl numbers [21]. A large Prandtl number reduces the flow to a pure poloidal field. In the present work, we have considered velocity patterns imposed by surface conditions rather than being the consequences of thermal convection in a homogeneous fluid. The presence of chaotic pathlines which are suspected in Fig. 5b indicates that poloidal flows driven by imposed motions do not behave as poloidal flows induced by thermal convection. It is however clear that, if they exist, the ergodic regions in pure poloidal flows are small and restricted to cell boundaries. In contrast, a more general flow such as that existing in the mantle leads to large areas of chaotic pathlines and to a turbulent exponential mixing even without explicit time dependence of the flow. This result agrees with the conclusions obtained for the first time by Bajer and Moffatt [19] for a general quadratic flow confined in a sphere. This explains why faster

stretching rates are observed in models with plates than without [12].

An important result of our study that should be remembered when interpreting geochemical data is best illustrated by Fig. 5d. In this case of two diverging plates we obtain apparently three reservoirs. The two unmixed (blue) reservoirs are in fact connected and belong to the same torus. The well-mixed (green to red) and the unmixed reservoirs are separated by impermeable boundaries. This is obtained in a situation where no density stratification and no viscosity variations are present in the convecting fluid. Transposing this model to the Earth, we see that all samples dragged above the diverging and transforming boundaries could have been sampling a shallow well-mixed mantle whereas hotspots might have sampled an isolated unmixed domain. It would have been erroneous to conclude that the underlying fluid was stratified or heterogeneous in its physical properties.

The mantle convection is certainly not at steady state. Mixing studies using 2-D time-dependent convection patterns have predicted that the upper mantle is homogenized by stirring within ~ 200 Myr. This is much shorter than the time-scale on which geochemical isotope systems evolve (e.g., Rb–Sr or Sm–Nd). The conclusions about the homogenization of the lower mantle are far less certain and depend on the amount of viscosity increase with depth [8]. Contrarily, the only study on 3-D time-dependent mantle convection (with poloidal flow) we are aware of, by Schmalzl et al. [14], concludes that 3-D convection is far less efficient than 2-D convection to mix the mantle. Their arguments agree with those of Davies [33]. In the 2-D case, the boundary layer instabilities have implicit sheet-like structures. They split the large-scale flow and generate stagnation points, yielding turbulent mixing. In the 3-D case, many instabilities have columnar structures which penetrate the large-scale flow without major disruption and give way to laminar mixing (zero Lyapunov exponents). If the conclusions of Schmalzl et al. [14] are correct, the mixing of the mantle due to the explicit time dependence of the convection may not be more efficient than that due to the very existence of plates.

Models of mantle dynamics agree on an increase in viscosity with depth in the mantle, the sluggish

lower mantle being one or two orders of magnitude more viscous. In that case, the toroidal energy of the mantle flow is mostly confined to the upper mantle and the toroidal/poloidal ratio decreases from ~ 1 in the asthenosphere to barely zero in the lower mantle [34,35]. This favors a pathline topology yielding a chaotic upper mantle on top of a quasi-regular lower mantle where independent more or less well-mixed reservoirs are present. The time dependence in the convection within the Earth will reinforce the differences between the mixing rates of the active upper mantle and the stiffer lower mantle. These speculations will have to be tested by studies with both time-dependent flows and toroidal/poloidal quasi equipartition to quantify the relative importance of these two ingredients for mantle mixing. At any rate, our findings show that previous studies restricted to the 2-D case did not capture one fundamental aspect of the physics of mantle mixing.

Acknowledgements

This study benefited from suggestions by and discussions with F. Albarède, U. Christensen, R. O'Connell, C. Gable and J. Schmalzl. **[RO]**

References

- [1] C.J. Allègre, Chemical geodynamics, *Tectonophysics* 81 (1982) 109–132.
- [2] A. Zindler, S. Hart, Chemical geodynamics, *Annu. Rev. Earth Sci.* 14 (1986) 493–571.
- [3] A.W. Hofmann, Chemical differentiation of the Earth: the relationship between mantle, continental crust, and oceanic crust, *Earth Planet. Sci. Lett.* 90 (1988) 297–314.
- [4] S. Hart, A. Zindler, Constraints on the nature and development of chemical heterogeneities in the mantle, in: W.R. Peltier (Ed.), *Mantle Convection, Plate Tectonics and Global Dynamics*, Gordon and Breach, New York, NY, 1989, pp. 261–387.
- [5] D. McKenzie, Finite deformation during fluid flow, *Geophys. J.R. Astron. Soc.* 58 (1979) 689–715.
- [6] N.R.A. Hoffman, D.P. McKenzie, The destruction of geochemical heterogeneities by differential fluid motions during mantle convection, *Geophys. J.R. Astron. Soc.* 82 (1985) 163–206.
- [7] M. Gurnis, G.F. Davies, Mixing in numerical models of mantle convection incorporating plate kinematics, *J. Geophys. Res.* 91 (1986) 6375–6395.
- [8] U. Christensen, Mixing by time-dependent convection, *Earth Planet. Sci. Lett.* 95 (1989) 382–394.
- [9] L.H. Kellogg, D.L. Turcotte, Mixing and the distribution of heterogeneities in a chaotically convecting mantle, *J. Geophys. Res.* 95 (1990) 421–432.
- [10] M. Manga, Mixing of heterogeneities in the mantle: effect of viscosity differences, *Geophys. Res. Lett.* 23 (1996) 403–406.
- [11] U. Christensen, A. Hoffmann, Segregation of subducted oceanic crust in the convecting mantle, *J. Geophys. Res.* 99 (1994) 19867–19884.
- [12] C.W. Gable, H.A. Stone, R.J. O'Connell, Chaotic mantle mixing: Time dependence is unnecessary, *Eos (Trans. Am. Geophys. Union)* 72 (1991) 269.
- [13] J. Schmalzl, G.A. Houseman, U. Hansen, Mixing properties of three-dimensional stationary convection, *Phys. Fluids* 7 (1995) 1027–1033.
- [14] J. Schmalzl, G.A. Houseman, U. Hansen, Mixing in vigorous time-dependent 3D convection and application to the Earth's mantle, *J. Geophys. Res.* 10 (1996) 21847–21858.
- [15] K.J. Whiteman, Invariants and stability in classical mechanics, *Rep. Prog. Phys.* 40 (1977) 1033–1069.
- [16] J.R. Cary, R.G. Littlejohn, Noncanonical Hamiltonian mechanics and its application to magnetic field line flow, *Ann. Phys.* 151 (1983) 1–34.
- [17] T. Dombre, U. Frisch, J.M. Greene, M. Hénon, A. Mehr, A.M. Soward, Chaotic streamlines in the ABC flows, *J. Fluid Mech.* 167 (1986) 353–391.
- [18] H.A. Kusch, J.M. Ottino, Experiments on mixing in continuous chaotic flows, *J. Fluid Mech.* 236 (1992) 319–348.
- [19] K. Bajer, H.K. Moffatt, On a class of steady confined Stokes flows with chaotic streamlines, *J. Fluid Mech.* 212 (1990) 337–363.
- [20] V. Toussaint, P. Carrière, F. Raynal, A numerical Eulerian approach to mixing by chaotic advection, *Phys. Fluids* 7 (1995) 2587–2600.
- [21] W. Arter, Nonlinear Rayleigh–Bénard convection with square planform, *J. Fluid Mech.* 152 (1985) 391–418.
- [22] Y. Ricard, C. Vigny, Mantle dynamics with induced plate tectonics, *J. Geophys. Res.* 94 (1989) 17543–17559.
- [23] B.H. Hager, R.J. O'Connell, Subduction zone dip angles and flow driven by plate motion, *Tectonophysics* 50 (1978) 111–133.
- [24] O. Čadež, Y. Ricard, Toroidal/poloidal partitioning and global lithospheric rotation during Cenozoic time, *Earth Planet. Sci. Lett.* 109 (1992) 621–632.
- [25] C. Lithgow-Berteloni, M.A. Richards, Y. Ricard, R.J. O'Connell, Toroidal–poloidal partitioning of Cenozoic and Mesozoic plate motions, *Geophys. Res. Lett.* 20 (1993) 375–378.
- [26] B.H. Hager, R.J. O'Connell, A simple global model of plate dynamics and mantle convection, *J. Geophys. Res.* 86 (1981) 4843–4867.
- [27] J.M. Ottino, *The Kinematics of Mixing: Stretching, Chaos and Transport*, Cambridge University Press, Cambridge, 1989.
- [28] A.J. Lichtenberg, M.A. Lieberman, *Regular and Chaotic Dynamics*, Springer, Berlin, 1992.

- [29] E. Ott, *Chaos in Dynamical Systems*, Cambridge University Press, Cambridge, 1993.
- [30] P. Olson, D.A. Yuen, D. Balsiger, Mixing of passive heterogeneities by mantle convection, *J. Geophys. Res.* 89 (1984) 425–436.
- [31] C.J. Allègre, D.L. Turcotte, Implications of a two-component marble-cake mantle, *Nature (London)* 323 (1986) 123–127.
- [32] G. Metcalfe, C.R. Bina, J.M. Ottino, Kinematic considerations for mantle mixing, *Geophys. Res. Lett.* 22 (1995) 743–746.
- [33] G.F. Davies, Comment on “Mixing by time-dependent convection”, by U. Christensen, *Earth Planet. Sci. Lett.* 98 (1990) 405–407.
- [34] C. Vigny, *Géologie et dynamique interne de la Terre*, Ph.D. Thesis, University of Paris-Sud, Orsay, 1986.
- [35] C.W. Gable, R.J. O’Connell, B.J. Travis, Convection in three dimensions with surface plates: generation of toroidal flow, *J. Geophys. Res.* 96 (1991) 8391–8405.